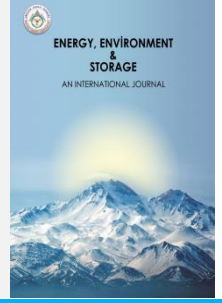




# Energy, Environment and Storage

Journal Homepage: [www.enenstrg.com](http://www.enenstrg.com)



## PYTHON BASED INVESTIGATION OF COMPRESSIBLE FLOW CALCULATIONS UNDER VARIABLE ATMOSPHERIC CONDITIONS

Makbule Esra SIRÇA<sup>1\*</sup>, Bilge ALBAYRAK ÇEPER<sup>2</sup> and Nafiz KAHRAMAN<sup>3</sup>

<sup>1\*</sup> Erciyes University, Faculty of Aeronautics and Astronautics, Astronautical Engineering Undergraduate Program, Kayseri, Türkiye, [makbuleesrasirca@gmail.com](mailto:makbuleesrasirca@gmail.com), ORCID: <https://orcid.org/0009-0000-3580-7902>

<sup>2</sup> Erciyes University, Faculty of Aeronautics and Astronautics, Astronautical Engineering, Kayseri, Türkiye, [balbayrak@erciyes.edu.tr](mailto:balbayrak@erciyes.edu.tr), ORCID: <https://orcid.org/0000-0001-5556-5170>

<sup>3</sup> Erciyes University, Faculty of Aeronautics and Astronautics, Astronautical Engineering, Kayseri, Türkiye, [nafiz@erciyes.edu.tr](mailto:nafiz@erciyes.edu.tr) ORCID: <https://orcid.org/0000-0002-8698-8632>

**ABSTRACT.** Flow and thrust calculations at supersonic speeds require intensive formulas and general assumptions, thus prolonging the preliminary design process. Today, the use of computer programs for aerodynamic design and analysis is inevitable in the development of aircraft. However, in this process, traditional calculation methods are mostly used. By performing the relevant calculations with a source code, time-consuming problems such as data extraction from tables, interpolation or calculation with formulas can be avoided. In this study, a computational tool was created in Python using the formulas contained in compressible flow theory. For the calculation, ISA (International Standard Atmosphere) and altitude values are first obtained from the user to determine the atmospheric conditions. These conditions are known to directly affect static conditions. Then, the data input of one of the selected parameters is made and the remaining parameters according to these input values are presented on the result screen together with the other outputs. These outputs were compared with NASA data and their accuracy was analysed. Two different configurations were created to examine the dependence of compressible flow calculations on atmospheric conditions. In the first one, constant ISA and different altitude values were analysed, while in the other one, constant altitude and different temperature deviations were evaluated. These evaluations revealed the sensitivity of the calculation results to atmospheric variables. The findings provide critical data on how to design and analyse aircraft under different operational conditions. This study, for the first time, provides calculations based on atmospheric variables, enabling them to efficiently obtain the values of parameters that depend on these data. This approach is an innovative contribution to the existing literature, expanding the body of knowledge on the analysis of compressible flows.

**Keywords:** Compressible Flow, Isentropic Flow, Shock Waves, Atmospheric Conditions, Python

**Article History:** Received:xxx; Revised: xxxx; Accepted:xxx; Availableonline: xxx (8 pt)

**Doi:**

### 1. INTRODUCTION

Isentropic flow is a reversible and adiabatic process with no energy losses. This type of flow is used to study ideal states in aerodynamics and thermodynamics [1]. Shock waves are waves that cause sudden changes in the velocity, pressure, temperature and density of the fluid. They are usually seen in fluids moving at high speeds [2]. Compressible flows occur when the Mach number is greater than 0.3 and under these conditions, the density and other thermodynamic properties of the fluid change significantly [3,4]. These

concepts are of critical importance in the fields of aerodynamics and gas dynamics and are used in a wide range of engineering applications [5,6]. One of the most common uses of compressible flows is in aerospace engineering. The aerodynamic design and performance analysis of such vehicles requires a detailed understanding of compressible flow dynamics [7]. Especially for vehicles flying at supersonic and hypersonic speeds, accurate modelling of shock waves and isentropic flows is of great importance [8]. Compressible flow calculations also play a

critical role in the design of propulsion systems such as rocket and jet engines. The nozzle designs used in rocket engines are based on isentropic flow principles to achieve maximum thrust [9]. Such engines involve gas dynamics operating at high speeds, and optimizing engine performance requires accurate application of compressible flow equations [10]. Another important application of compressible flows is wind tunnel experiments [11]. High speed wind tunnels are used in aerospace engineering tests [12] and compressible flow equations are needed to accurately model the flow conditions in these tunnels [13]. These experiments are used to evaluate the aerodynamic performance and stability of aircraft and spacecraft [14]. Ratios such as  $P/P_t$ ,  $T/T_t$ , etc. used in compressible flow calculations are determined based on Mach and gamma numbers, and in NASA studies in the literature, it was sufficient to know only the Mach number to calculate these ratios [15]. In other words, variable atmospheric conditions such as altitude and ISA were not needed. However, besides the fact that the variability of atmospheric conditions is of great importance for weather forecasts and climate models [13], taking these conditions into account allows for more accurate modelling and calculation of static parameters. This allows compressible flow calculations to obtain more reliable results under variable atmospheric conditions [4]. It is noted that the values of the static parameters can vary greatly under these conditions. Therefore, accurate static parameters are critical for aircraft performance and safety. Accurate determination of these values leads to significant improvements in flight dynamics and aircraft design [7]. In recent years, significant progress has been made in the development of numerical solvers for compressible and incompressible flows within the field of computational fluid dynamics (CFD). In his master's thesis, Kerem Denk developed a two-dimensional, pressure-based Navier–Stokes solver for both compressible and incompressible flows [16]. Similarly, Emre Kara, in his doctoral dissertation, proposed a pressure-based solver for two-dimensional compressible and incompressible flows [17]. In another related study, Semih Akkurt developed a parallel finite volume solver for compressible flows operating on unstructured meshes as part of his master's thesis [18]. The current study aims to be integrated with these solvers and similar CFD development frameworks to achieve more accurate and reliable results. The use of Python, in particular, has become increasingly prevalent in recent years due to the rise of Python-based compressible flow solvers [19,20], which have significantly improved both the accuracy and computational efficiency of such simulations. Among these, the CompAero library [21] stands out as a fundamental reference for modeling compressible aerodynamic analyses using Python. In this study, the impact of atmospheric conditions on compressible flow behavior is systematically analyzed through two different configurations; novel methods are proposed to model and calculate these effects with greater accuracy.

## 2. MATERIALS AND METHODS

### 2.1 Standard Atmosphere Model

For the design process and performance of aircraft, it is important to know the altitude-dependent change

information of parameters such as temperature and pressure [22]. Therefore, it is necessary to study the atmosphere at a specific time and place. However, the fact that the real atmosphere is never constant is an obstacle. Therefore, a hypothetical model was used and called the “standard atmosphere”. In the 1920s, the first standard models were developed independently in both Europe and the USA. By 1952, the models were compared and the differences were minimized and a model accepted by the International Civil Aviation Organization (ICAO) was created. The ICAO Standard Atmosphere model was also officially accepted by NACA in the same year [23]. Finally, air -assumed to behave as a perfect gas in the ISA model- can be modeled as follows. In Equations (1)–(6), the temperature  $T$  is expressed in degrees Celsius ( $^{\circ}\text{C}$ ), the altitude  $h$  in kilometers (km), and the pressure  $P$  in kilopascals (kPa). Temperature and pressure calculation at altitude up to the troposphere; (0-11 km)

$$T = 15.04 - (0.00649 \times h) \quad (1)$$

$$P = 101.29 \times \left[ \frac{T+273.15}{288.08} \right]^{5.256} \quad (2)$$

Lower Stratosphere; (11-20 km)

$$T = -56.46 \quad (3)$$

$$P = 22.65 \times e^{(1.73-0.000157 \times h)} \quad (4)$$

Upper Stratosphere; (20-47 km)

$$T = -131.21 + (0.00299 \times h) \quad (5)$$

$$P = 2.488 \times \left[ \frac{T+273.15}{216.6} \right]^{-11.388} \quad (6)$$

The given ISA model was used as a reference to compare real atmospheric conditions and the performance of the respective aircraft [24]. In addition to this ISA model, the temperature deviation was also included in the calculations, expressed as  $\pm \Delta\text{ISA}$ , to obtain the actual temperature. In this way, the accuracy of the study was increased by running it with real atmospheric data. This is an innovative approach to the literature and allows for a more detailed analysis of the computational results.

### 2.2 Compressible Flow

The characteristic equations used in the Compressible Flow calculations were compiled from the relevant literature [15,25] and given as equations. These equations were used in Python code and the calculations for the 2 configurations to be examined were performed through this Python code. It is known that entropy remains constant for isentropic processes [26]. From this, we derive the most general form of the isentropic equations. In Equations (7)-(18), the temperature  $T$  and total temperature  $T_t$  are given in degrees Celsius ( $^{\circ}\text{C}$ ). The pressure  $P$  and total pressure  $P_t$  are expressed in kilopascals (kPa). The density terms  $\rho$  and  $\rho_t$  are measured in kilograms per cubic meter ( $\text{kg}/\text{m}^3$ ). The areas  $A$  and  $A^*$  are in square meters ( $\text{m}^2$ ), although they may appear dimensionless in certain ratio-based expressions. The Mach numbers ( $M$ ,  $M_1$ ,  $M_2$ ) are nondimensional quantities. Angular terms such as the

Prandtl-Meyer function ( $\nu$ ), Mach angle ( $\mu$ ), shock wave angle ( $\alpha$ ), and deflection angle ( $\theta$ ) are expressed in degrees ( $^\circ$ ). Since most of the equations are ratio-based, many of the resulting terms are dimensionless.

$$\frac{T_t}{T} = \left[ \frac{P_t}{P} \right]^{\frac{\gamma-1}{\gamma}} = \left[ \frac{\rho_t}{\rho} \right]^{\gamma-1} \quad (7)$$

$$\frac{T}{T_t} = \left[ 1 + \frac{\gamma-1}{2} M^2 \right]^{-1} \quad (8)$$

$$\frac{A}{A^*} = \left[ \frac{\gamma+1}{2} \right]^{\frac{-\gamma+1}{2(\gamma+1)}} = \frac{\left[ 1 + \frac{\gamma-1}{2} M^2 \right]^{\frac{\gamma+1}{2(\gamma-1)}}}{M} \quad (9)$$

The subscript “t” in the equations stands for “total conditions”. The starred conditions are when the Mach number is equal to one. As seen in the equations, once the Mach number is determined, all other parameters are also determined. Likewise, by determining one of the flow parameters (e.g. Temperature Ratio), the Mach number is found and the other parameters can be calculated [15].

The analysis of shock waves is done using Rankine-Hugoniot relations, and these relations play a critical role in understanding the physical and mathematical effects of shock waves. Also, the total temperature remains constant throughout the normal shock [8]. Normal shock equations are given below:

$$M_2^2 = \frac{(\gamma-1)M_1^2+2}{2\gamma M_1^2-(\gamma-1)} \quad (10)$$

$$\frac{T_2}{T_1} = \frac{[2\gamma M_1^2-(\gamma-1)][(\gamma-1)M_1^2+2]}{(\gamma+1)^2 M_1^2} \quad (11)$$

$$\frac{P_2}{P_1} = \frac{2\gamma M_1^2-(\gamma-1)}{(\gamma+1)} \quad (12)$$

$$\frac{\rho_2}{\rho_1} = \frac{(\gamma+1)M_1^2}{(\gamma-1)M_1^2+2} \quad (13)$$

$$\frac{P_{t2}}{P_{t1}} = \left[ \frac{(\gamma+1)M_1^2}{(\gamma-1)M_1^2+2} \right]^{\frac{\gamma}{\gamma-1}} \left[ \frac{(\gamma+1)}{2\gamma M_1^2-(\gamma-1)} \right]^{\frac{1}{\gamma-1}} \quad (14)$$

$$\nu = \sqrt{\frac{\gamma+1}{\gamma-1}} \tan^{-1} \sqrt{\frac{\gamma-1}{\gamma+1} (M_1^2 - 1)} - \tan^{-1} \sqrt{M_1^2 - 1} \quad (15)$$

$$\mu = \sin^{-1} \left[ \frac{1}{M_1} \right] \quad (16)$$

Oblique shock calculations;

$$\cot(a) = \tan(s) \left[ \frac{(\gamma+1)M_1^2}{2(M_1^2 \sin(s)^2 - 1)} - 1 \right] \quad (17)$$

$$M_2^2 (\sin(s-a))^2 = \frac{(\gamma-1)M_1^2 (\sin(s))^2 + 2}{2\gamma M_1^2 (\sin(s))^2 - (\gamma-1)} \quad (18)$$

The values of the ratios  $P_2/P_1$ ,  $T_2/T_1$ , etc. in the flow of a perfect gas for an oblique shock wave were determined from normal shock relations, provided that  $M_1 \sin(s)$  was used instead of  $M_1$  and the static temperature  $T_1$  just upstream of the shock wave was the same as the normal shock wave for an oblique shock wave [15].

### 2.3 Method

For this calculation, atmospheric conditions were first determined by taking ISA and altitude. In this way, it was possible to examine the situation under arbitrarily variable atmospheric conditions. Then, the data input of a selected parameter such as  $M$ ,  $P$ ,  $M_2$ ,  $T/T_t$ , etc. was made and the remaining parameters according to these input values were presented on the result screen together with the other outputs. Python language was used in the study. Thanks to popular libraries such as Pandas and NumPy, data manipulation and visualization is made extremely easy [27, 28]. The interface obtained when the code is run is given in Figure 1. Here the ISA and altitude values are variable. This allowed the current atmospheric conditions to be provided as input. Then one of the parameters was selected and its value or values were entered. If only one value is entered, the result screen is shown in Figure 2, and if more than one value is entered, the result screen is shown in Figure 3.

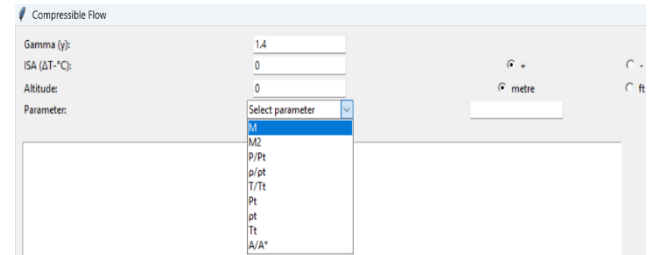


Fig. 1. Application Interface

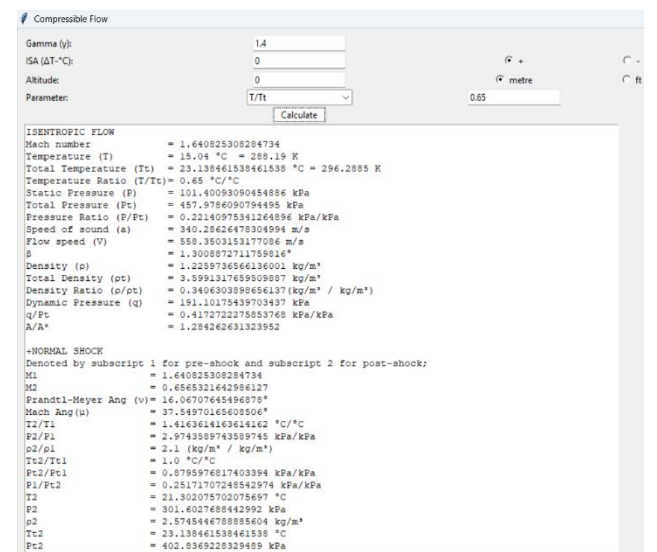


Fig. 2. An example of an output screen when entering a single value

h	0	0	0	0
ISA	0	0	0	0
M	0.1	1	10	100
a (m/s)	340.3	340.3	340.2863	340.286265
V (m/s)	34.03	340.3	3402.863	34028.6265
$\beta$ (°)	0.995	0	9.949874	99.9949999
T (°C)	15.04	15.04	15.04	15.04
Tt (°C)	15.07	18.05	315.84	30095.04
T/Tt	0.998	0.833	0.047619	0.00049975
P (kPa)	101.4	101.4	101.4009	101.400931
Pt (kPa)	102.1	191.9	4303378	3.6342E+13
P/Pt	0.993	0.528	2.36E-05	2.7902E-12
$\rho$ (kg/m <sup>3</sup> )	1.226	1.226	1.225974	1.22597366
$\rho t$ (kg/m <sup>3</sup> )	1.232	1.934	2477.59	219583074
$\rho/\rho t$	0.995	0.634	0.000495	5.5832E-09
q (kPa)	0.71	70.98	7098.065	709806.516
q/Pt	0.007	0.37	0.001649	1.9531E-08
A/A*	5.822	1	535.9375	46365775.5
M2	-	1	0.387575	0.37806165
$v$ (°)	-	0	102.3163	127.589813
$\mu$ (°)	-	90	5.73917	0.57296734
P2 (kPa)	-	101.4	11813.21	1182993.96
P2/P1	-	1	116.5	11666.5
$\rho 2$ (kg/m <sup>3</sup> )	-	1.226	7.005564	7.35216586
$\rho 2/\rho 1$	-	1	5.714286	5.9970015
T2 (°C)	-	15.04	306.628	29258.6487
T2/T1	-	1	20.3875	1945.38888
Tt2/Tt	-	1	1	1
Pt2 (kPa)	-	191.9	13102.72	1305644.19
Pt2/Pt1	-	1	0.003045	3.5927E-08

Fig. 3. An example of an output screen when multiple values are entered

To check the accuracy of the program, the results were compared with the results published by NASA in its 1135 report, and the results were found to be identical [15]. However, in this study, unlike NASA's study, the calculations were not limited to ratios. Thanks to these calculations made by taking into account the variations in atmospheric conditions, static and total conditions were evaluated in addition to the ratios, thus enabling us to present these static and total conditions as results. With this method, a more comprehensive and flexible analysis was presented, taking into account atmospheric variables.

### 3. DISCUSSION, CONCLUSION, AND RECOMMENDATIONS

#### 3.1 Discussion

Basic parameters such as temperature (T), pressure (P) and density ( $\rho$ ) vary depending on atmospheric conditions. And these parameters have a direct impact on aircraft performance, engine efficiency and flight safety [29]. The effect of ISA and altitude on these values is critical to understanding how atmospheric conditions change flight dynamics. Variations in temperature and pressure between these layers at different rates have decisive effects on the performance of aircraft [30]. For example, at higher altitudes, lower density and pressure values create less lift on aerodynamic surfaces, while changes in the speed of sound can affect shock wave generation [31]. A detailed analysis of these factors helps to determine operational limits during the aircraft design process [29].

In this study, the effect of atmospheric conditions on compressible flow calculations with different configurations was discussed. In the first configuration, the results were evaluated at constant ISA (0) at different altitudes (0, 10,000, 20,000, 40,000 meters). In the other

configuration, the effects of atmospheric parameters on airflow at sea level (0 m) at different ISA deviations (-20, -10, +10 and +20 °C) were analysed. The altitudes selected in the study represent altitudes in different layers of the atmosphere such as troposphere and stratosphere. Static values related to these configurations are calculated with Python code and given in Tables 1 and 2.

Table 1 Configuration 1; altitude-dependent static values only

h(m)	ISA(°C)	T(°C)	a (m/s)	$\rho$ (kg/m <sup>3</sup> )	P (kPa)
0	0	15.04	340.28626	1.2259736	101.40093
10000	0	-49.86	299.5295	0.413771	26.516206
20000	0	-56.46	295.0695	0.0889185	5.529845
40000	0	-11.61	324.17089	0.00388	0.2913066

Table 2 Configuration 2; static values connected to ISA only

h(m)	ISA(°C)	T(°C)	a (m/s)	$\rho$ (kg/m <sup>3</sup> )	P (kPa)
0	-20	-4.96	328.266	0.90263	69.47591
0	-10	5.03999	334.33	1.05485	84.21983
0	10	25.04	346.1398	1.41756	121.3161
0	20	35.04	351.8959	1.63126	144.2864

The other parameters affected by these variations also depend on the Mach number. At higher speeds, the effects of these parameters become more complex. Therefore, in order to investigate the variation in these parameters, the study evaluated parameters such as total temperature, flow/vehicle velocity and dynamic pressure over a wide range of Mach numbers under different altitude and ISA conditions. Mach number dependent graphs were created and presented between Figure 4 and Figure 9. The Mach number range considered in the study was chosen as 0-5 in order to evaluate how aircraft behave over a wide speed spectrum, covering subsonic, supersonic and hypersonic flight regimes. In this way, these calculations, performed at different altitudes, at different temperature deviations and over a wide range of Mach numbers, provide vital data for predicting challenges in aircraft design and developing optimal solutions to these challenges [29].

The variation in sound speed and temperature for different configurations are given in Tables 1 and 2. Depending on the atmospheric conditions, the static temperature affects the speed of sound and hence the Mach number. This in turn affects whether the flight is subsonic or supersonic. For example, due to the decrease in the speed of sound at high altitudes, an aircraft flying at the same absolute speed reaches a higher Mach number. This means that supersonic flight will occur earlier (at lower absolute speed) at higher altitudes. This can be advantageous in terms of fuel efficiency and engine design, provided the engine is designed for high altitude conditions. However, due to the low temperatures, changes in material strength and aerodynamic structures need to be considered.

Figure 4 shows a graph of total temperature and aftershock temperature as a function of Mach number under different atmospheric conditions. The graph shows that at higher

altitudes, the total temperature generally starts low initially, while at lower altitudes, higher total temperatures are observed initially. This is due to the higher air temperature closer to sea level. When the curves such as  $T_t$ ,  $T_t-10$ ,  $T_t+20$  in the graph are analysed, different total temperature values are observed depending on the ISA values. A positive temperature deviation starts the total temperature higher than it actually is, while a negative temperature deviation starts it at lower temperatures. As the Mach number increases, it is observed that the total temperature increases in absolute terms in all total temperature curves. This is because as the Mach number increases, compressible flow effects come into play and convert

kinetic energy into temperature [32]. Especially after Mach 2, it is seen that the curves change rapidly, which shows that the temperature change is more pronounced at high speeds. Shock waves and the aerodynamic losses caused by these waves are related to temperature. The effect of shock waves during supersonic flights results in heating and pressure increase on the surface of the aircraft [33]. The increase in Mach number significantly increases the intensity of the shock and the temperature variation. The temperature deviation significantly changed the temperature changes after the shock. With all these, it is generally understood from the graph how much altitude, temperature deviation and speed affect the static and total temperature.

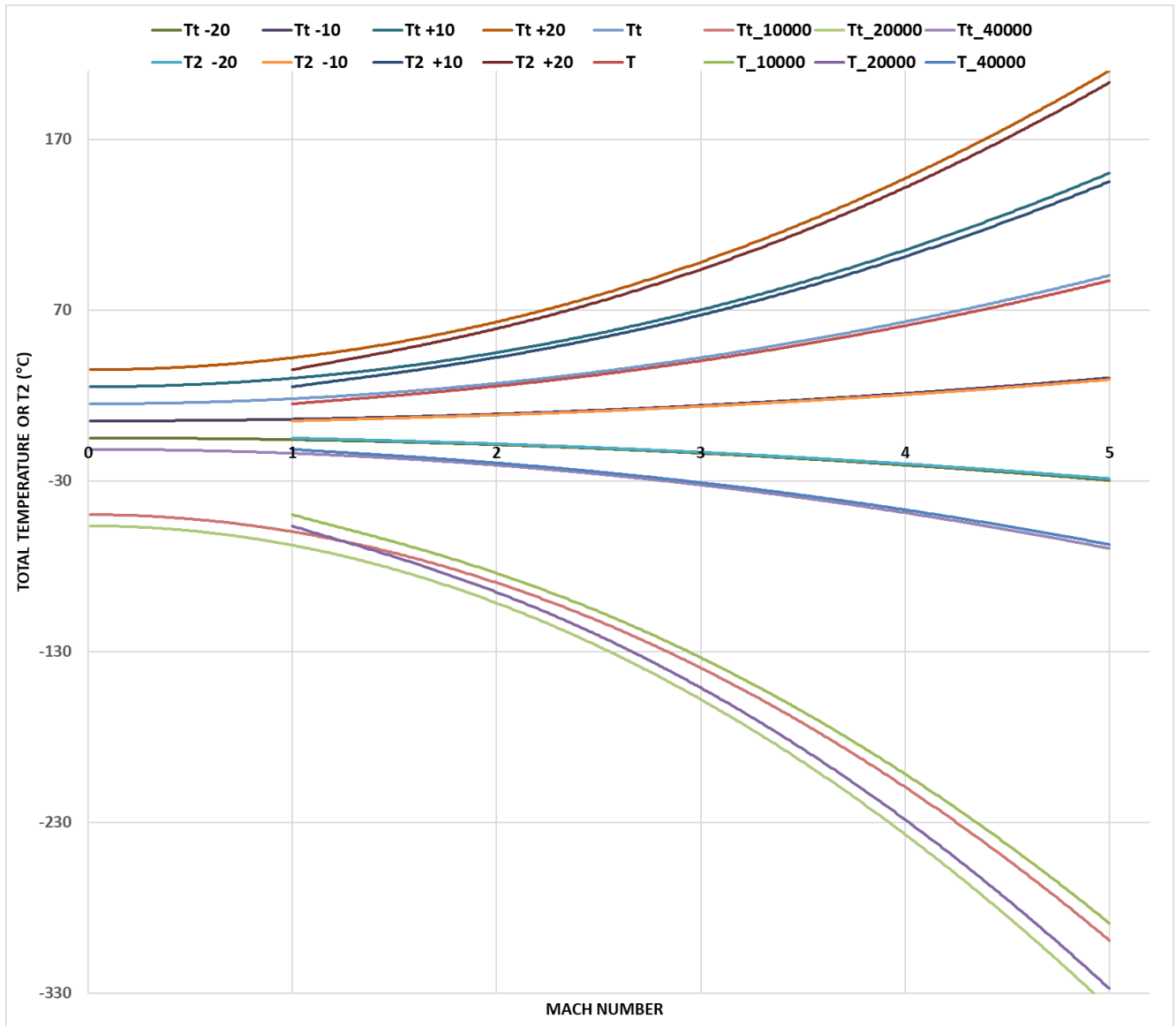


**Fig. 4.** Mach, Total Temperature and Static Temperature Graph after Shock for Configuration 1 and 2

Figure 5 shows how the static and total pressure changes with ISA, altitude conditions and Mach numbers after shock formation. The shock wave causes a sudden increase in pressure. At low altitudes, the higher air density causes air compression during the shock wave to create a larger pressure increase. At high altitudes, the air density is lower, so the post-shock pressure increases less. However, pressure spikes were still observed with increasing Mach

number. The lower density at high altitudes caused the pressure increase to be more controlled. Warmer air has a lower density, which can reduce the rate of increase in post-shock pressure. But there was still a post-shock pressure increase at supersonic speeds. Since cooler air is denser, the aftershock pressure is higher. This means that there is more compression during the shock wave, which causes the pressure to increase at a greater rate.

The shock wave abruptly reduces the velocity of the flow while increasing other parameters such as pressure, temperature and density. But since these sudden changes are not reversible, energy loss occurs in the flow. This energy loss causes a drop in total pressure. In the graph, the total pressure in the pre-shock flow is generally high, whereas in the post-shock flow it decreases due to friction and the effect of the shock. It was observed that the higher

the Mach number before the shock, the greater the total pressure loss after the shock. There is a sudden loss of energy in the flow during the shock wave. These losses are not reversible and the total pressure of the flow is affected by this energy loss. Shock waves usually cause losses due to friction and viscosity. These losses result in the conversion of some of the energy of the flow into heat, which leads to a drop in the total pressure [33].

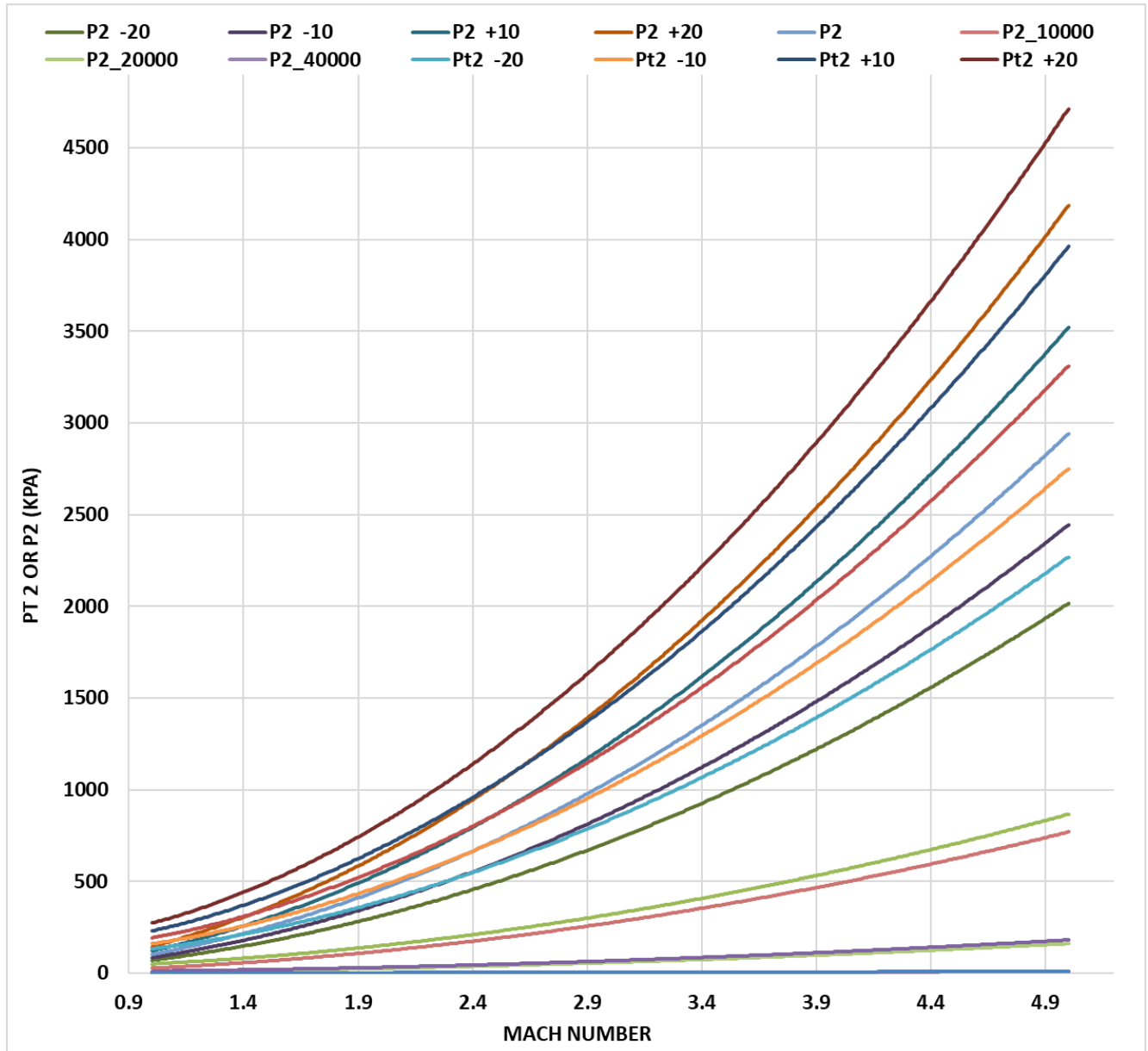
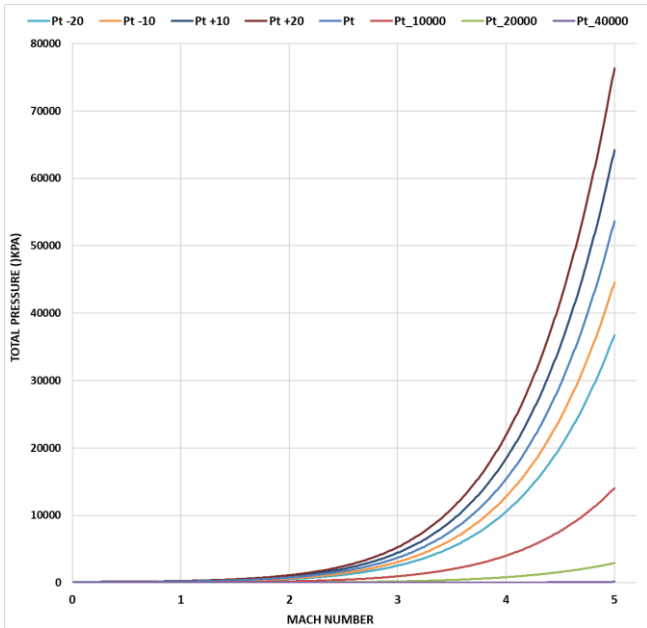


Fig. 5. Mach, Post-Shock Static and Total Pressure Graph for Configurations 1 and 2

Figure 6 shows how the total pressure changes with ISA, altitude conditions and Mach numbers. At lower Mach numbers (between 0 and 1), the increase in total pressure is limited at low speed. This is associated with the velocity regime in which the flow can be considered incompressible. At higher Mach Numbers (especially Mach 3 and beyond), the total pressure increases rapidly as the Mach number increases. Here, it is seen that in the supersonic regime, where the flow becomes compressible, the total pressure increases rapidly due to the effect of shock waves and compression.

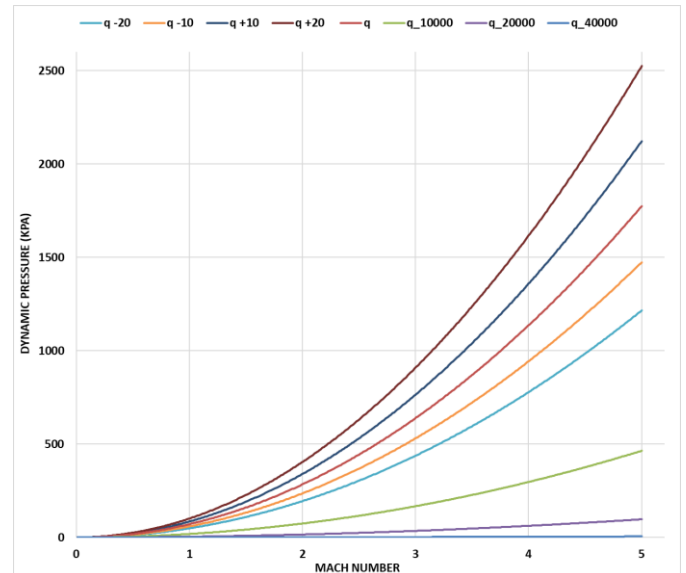
In the graph, the total pressure varies at different altitudes. While the highest total pressure values are reached at sea level (approximately 0 meters), these values decrease as the altitude increases. Especially at higher altitudes, the total pressure remains lower. And even if the Mach number increases, the increase in total pressure varies less at high altitudes than at sea level. This is due to the decrease in static pressure with increasing altitude as given in Table 1. Since the air density is lower at higher altitudes, the total pressure naturally decreases. At sea level, the total pressure is considerably higher than the total pressure at other

altitudes and rises much faster with the increase in Mach number. The high atmospheric pressure and density at sea level further increases the total pressure at high speeds. Where the temperature deviation is high, the total pressure is higher than where the temperature deviation is low. In a warm air environment, the total pressure is higher than in other ISA conditions. This is because the air is less dense when the temperature increases. This increases the compression of the flow and has an effect on the total pressure. In colder air, the total pressure is lower. Since cold air is denser, the same Mach number results in lower total pressure.



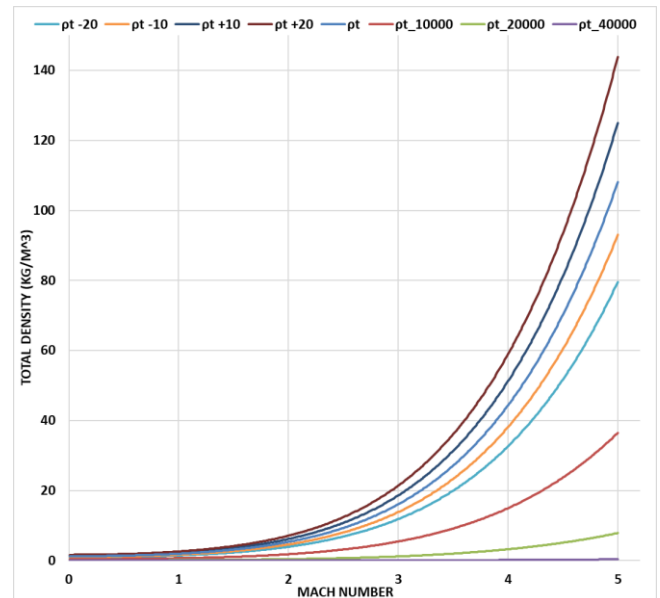
**Fig. 6.** Mach, Total Pressure Graph for Configurations 1 and 2

Figure 7 shows how the dynamic pressure varies with ISA, altitude conditions and Mach numbers. The dynamic pressure increase is relatively slow at low speeds where the flow can be considered incompressible. From Mach 3 onwards, a rapid increase in dynamic pressure is observed. This is due to the increase in the kinetic energy of the air flow as it accelerates. In this regime, the air becomes compressible and the pressure forces acting on the surface of the aircraft increase significantly. It is observed that the dynamic pressure decreases with increasing altitude. At higher altitudes, the density of the air is lower, so the dynamic pressure reaches lower values at the same Mach number. Different ISA values also affect the dynamic pressure. In warmer air conditions, the dynamic pressure is higher than in other conditions. Although warmer air is less dense, the increase in kinetic energy compensates for this and the dynamic pressure increases rapidly as the Mach number increases. In colder air, the air is denser, so the dynamic pressure is lower at the same speed. Because the air is denser, as the Mach number increases, the dynamic pressure remains lower than in other temperature conditions.



**Fig. 7.** Mach, Dynamic Pressure Graph for Configurations 1 and 2

The change in total density at different ISA, altitude and Mach numbers is given in Figure 8. Since these effects change the static temperature, they also change the total density. It can be seen from the graph that the temperature deviation changes the density in a directly proportional way. As the temperature increases, the density of the air decreases because warmer air expands and contains fewer molecules. In colder conditions, the density increases. As altitude increases, atmospheric pressure and temperature decrease, leading to a decrease in air density.



**Fig.8.** Mach, Total Density Plot for Configurations 1 and 2

The change in static density after the shock at different ISA, altitude and Mach numbers is presented in Figure 9. While the static density before the shock is independent of Mach number, the static density after the shock undergoes significant changes due to the effect of shock waves in compressible flows. While the flow velocity decreases during the shock, the pressure increases after the shock, leading to an increase in density. Despite the increased

pressure and temperature values after the shock, the density was more affected by the increase in pressure [34]. It is observed that the density decreases rapidly with increasing altitudes. The temperature deviation changed the total density in a directly proportional manner.

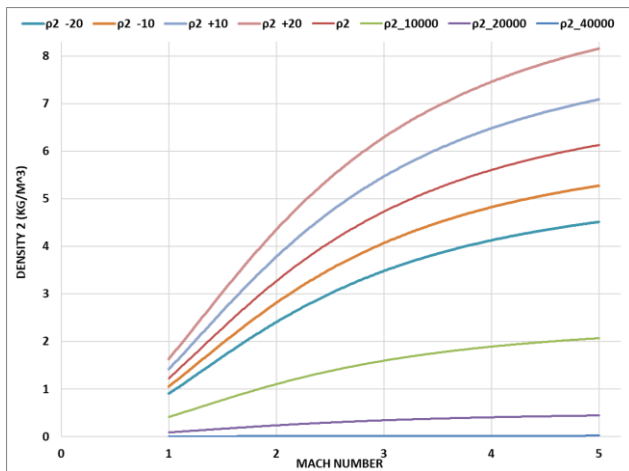


**Fig. 9.** Mach, Post-Shock Density Graph for Configurations 1 and 2

### 3.2 Conclusion and Recommendations

As can be understood from all these findings, it was determined that ignoring the atmospheric conditions led to data that did not match the actual values found in the current conditions. This is expected to cause problems in the design and analysis processes. For this design and analysis process, compressible flow parameters are of critical importance for performance-based design of engines and compressors [35], air intake and wing designs [36,37], in short, in all cases that directly affect the aerodynamic and structural design of the aircraft [38]. This is because flow regimes and aerodynamic forces can change depending on the compressibility effects of the flow [38]. While the variation of the stress acting on the aircraft affects the material selection [39], the varying thermal loads also create a material selection based on the resistance of the aircraft to thermal stresses. Total temperature information is critical for the calculation of thermal expansion and deformation [40]. This study can be integrated into computational fluid dynamics (CFD)-based software to enable more comprehensive analyses and serve as a foundation for future research.

### REFERENCES

- [1] Y. A. Çengel and M. A. Boles, *Thermodynamics: An Engineering Approach*, 5th ed., New York, NY, USA: McGraw-Hill, 2006.
- [2] J. E. Marsden and M. J. Hoffman, *Elementary Classical Analysis*, 2nd ed., vol. 37, Texts in Applied Mathematics. New York, NY, USA: Springer, 1993
- [3] A. Terenzi, *Flow Analysis for Hydrocarbon Pipeline Engineering*. Houston, TX, USA: Gulf Professional Publishing, 2022.
- [4] F. M. White and J. Majdalani, *Viscous Fluid Flow*, 3rd ed. New York, NY, USA: McGraw-Hill, 2006.
- [5] R. H. Chen, *Foundations of Gas Dynamics*. Cambridge, U.K.: Cambridge University Press, 2017.
- [6] J. W. Slooff and W. Schmidt, *Computational Aerodynamics Based on the Euler Equations, L'aérodynamique numérique à partir des équations d'Euler*, 1994.
- [7] H. W. Liepmann and A. Roshko, *Elements of Gasdynamics*. Mineola, NY, USA: Courier Corporation, 2001.
- [8] J. D. Anderson, *Modern Compressible Flow: With Historical Perspective*. New York, NY, USA: McGraw-Hill, 1990.
- [9] P. G. Hill and C. R. Peterson, *Mechanics and Thermodynamics of Propulsion*, 2nd ed. Reading, MA: Addison-Wesley, 1992.
- [10] G. P. Sutton and O. Biblarz, *Rocket Propulsion Elements*, 8th ed. Hoboken, NJ: John Wiley & Sons, 2011.
- [11] J. B. Barlow, W. H. Rae, and A. Pope, *Low-Speed Wind Tunnel Testing*, 3rd ed. Hoboken, NJ: John Wiley & Sons, 1999.
- [12] A. Pope and K. L. Goin, *High-Speed Wind Tunnel Testing*, 2nd ed. New York, NY: John Wiley & Sons, 1965.
- [13] S. B. Pope, *Turbulent Flows*. Cambridge, U.K.: Cambridge Univ. Press, 2000.
- [14] ASCE Aerospace Div. Task Comm. on Wind Tunnel Studies of Buildings and Structures, "Wind-Tunnel Studies of Buildings and Structures," *J. Aerosp. Eng.*, vol. 9, no. 1, pp. 19–36, 1996.
- [15] Ames Research Staff, "Equations, Tables, and Charts for Compressible Flow" NACA Report No. 1135, Moffett Field, CA: Ames Aeronautical Laboratory, 1953.
- [16] K. Denk, "Development of a Pressure-Based Solver for Both Incompressible and Compressible Flows", M.S. thesis, Dept. of Mechanical Engineering, Middle East Technical Univ., Ankara, Türkiye, 2007.
- [17] E. Kara, "Development of a Navier Stokes Solver for Compressible Flows on Cartesian Grids with Aerodynamics Applications", Ph.D. thesis, Dept. of Mechanical Engineering, Gaziantep Univ., Gaziantep, Türkiye, 2015.
- [18] S. Akkurt, "A Parallel Unstructured Finite Volume Method with an Efficient Edge-Based Data Structure for

Compressible Flows”, M.S. thesis, Fen Bilimleri Enstitüsü, Istanbul Technical Univ., İstanbul, Türkiye, 2018

[19] H. Wen, D. Liu, G. Baker, and M. Capecelatro, “Introducing JANC: A High-Performance Python-Based Solver for Compressible Reacting Flows,” *Quantum Zeitgeist*, 2024. [Online]. Available: <https://quantumzeitgeist.com/introducing-janc-a-high-performance-python-based-solver-for-compressible-reacting-flows>.

[20] A. K. Verma, “A Python-Based Tool for Constructing Observables from the DSN’s Closed-Loop Archival Tracking Data Files,” *SoftwareX*, 2022, doi:10.1016/j.softx.2022.101190

[21] R. M. Cummings, “CompAero: A Compressible Aerodynamics Python Library,” *GitHub Repository*, 2022. [Online]. Available: <https://github.com/Rigel09/CompAero>.

[22] E. İnger, *Roket ve Füze Mühendisliği*. İstanbul, Turkey: Palme Publishing, 2010.

[23] T. A. Talay, *Introduction to the Aerodynamics of Flight*, NASA-SP-367, 1975.

[24] Airbus S.A.S., *Getting to Grips with Aircraft Performance*, vol. 2(295), pp. 11–16, Blagnac, France: Customer Services, 2002.

[25] J. Anderson, *Fundamentals of Aerodynamics*, McGraw-Hill US Higher Ed, 2023.

[26] R. G. Maev and V. Leshchynsky, *Introduction to Low Pressure Gas Dynamic Spray: Physics and Technology*, John Wiley & Sons, 2009.

[27] T. J. Pollard, A. E. Johnson, J. D. Raffa, and R. G. Mark, “Tableone: An Open Source Python Package for Producing Summary Statistics for Research Papers,” *JAMIA Open*, vol. 1, no. 1, pp. 6–11, 2018.

[28] P. Gupta and A. Bagchi, *Essentials of Python for Artificial Intelligence and Machine Learning*, Springer, 2024.

[29] S. M. Yahya, *Fundamentals of Compressible Flow with Aircraft and Rocket Propulsion*, New Delhi, India: New Age International Publishers, 2014.

[30] U.S. Atmosphere, *U.S. Standard Atmosphere*, Washington, DC: National Oceanic and Atmospheric Administration (NOAA), 1976.

[31] R. Courant and K. O. Friedrichs, *Supersonic Flow and Shock Waves: A Manual on the Mathematical Theory of Non-linear Wave Motion*, vol. 21, New York, NY, USA: Interscience Publishers, 1948.

[32] M. A. Saad, *Compressible Fluid Flow*. Englewood Cliffs, NJ, USA: Prentice-Hall Inc., 1985,

[33] R. A. Graham, R. Cberet, F. G. Eden, and G. Britain, *High-Pressure Shock Compression of Condensed Matter*. New York, NY, USA: Springer-Verlag, 1995.

[34] A. Sasoh, *Compressible Fluid Dynamics and Shock Waves*. Singapore: Springer, 2020.

[35] J. D. Mattingly, *Aircraft Engine Design*. Reston, VA, USA: AIAA, 2002.

[36] A. Sóbester, “Tradeoffs in Jet Inlet Design: A Historical Perspective,” *Journal of Aircraft*, vol. 44, no. 3, pp. 705–717, 2007.

[37] R. J. Re, “An Investigation of Several NACA 1 Series Axisymmetric Inlets at Mach Numbers from 0.4 to 1.29,” NASA-TM-X-2917, 1974.

[38] N. Krasnov, *Fundamentals of Theory Aerodynamics of an Airfoil and a Wing*, Moscow, USSR: MIR Publishers, 1985.

[39] T. H. G. Megson, *Introduction to Aircraft Structural Analysis*, Oxford, UK: Butterworth-Heinemann, 2013.

[40] W. J. Bräunling, *Brennkammer. Flugzeugtriebwerke: Grundlagen, Aero-Thermodynamik, Ideale und Reale Kreisprozesse, Thermische Turbomaschinen, Komponenten, Emissionen und Systeme*, Wiesbaden, Germany: Springer Vieweg, 2015